JM PAPERS

A viscous continuum theory of sea ice motion based on stochastic floe dynamics

S. Toppaladoddi

School of Mathematics, University of Leeds, Leeds LS2 9JT, UK
Corresponding author: S. Toppaladoddi, s.toppaladoddi@leeds.ac.uk

In this study, we obtain the continuum equations of Arctic sea ice motion starting from the dynamics of a single floe and show that the rheology that emerges from floe–floe interactions is viscous – as conjectured by Reed and Campbell (*J. Geophys. Res.*, vol. 67 (1), 1962, pp. 281–297). The motion of the floe is principally driven by the wind and ocean currents and by inelastic collisions with the neighbouring floes. A mean-field representation of these collisions is developed, neglecting any changes in the floe thickness due to thermal growth and mechanical deformation. This mean-field representation depends on the state of the ice cover, and is expressed in terms of ice concentration and mean thickness. The resulting Langevin equation for the floe velocity, or the corresponding kinetic equation (Kramers–Chandrasekhar equation (KCE)) for its probability density, provides a complete description of the floe's motion. We then use the floe-scale dynamics to obtain a continuum description of sea ice motion through a Chapman–Enskog analysis of the KCE. The local equilibrium solution to the kinetic equation is found to be the Laplace distribution, in qualitative agreement with observations. Our approach also allows us to establish the dependence of pressure and shear viscosity of the ice cover on ice concentration and mean thickness. Lastly, we show that our results resolve a conflict associated with the choice of the value of shear viscosity in previous idealised numerical studies of Arctic sea ice motion.

Key words: sea ice

1. Introduction

The importance of the Arctic sea ice cover in the climate system stems primarily from its influence on the Earth's radiation budget, which it exerts through its relatively large albedo (Kwok & Untersteiner 2011). Despite its importance, predicting changes in the ice cover accurately, subject to prescribed forcings, still remains challenging. One of the principal

challenges associated with making this prediction is related to the dynamics of the ice cover (Rothrock 1975*a*; Kwok & Untersteiner 2011; Rampal *et al.* 2011; Fox-Kemper *et al.* 2021).

The ice cover is not continuous, but is made up of a very large number of floes of different shapes, sizes and thicknesses (Thorndike *et al.* 1975; Rothrock & Thorndike 1984). It can be inferred from field and satellite observations that sea ice behaves differently at different length scales: at the scale of an individual floe it moves like a deformable solid body (Parmerter 1975; Vella & Wettlaufer 2008), but at much larger scales it moves like a highly viscous fluid (Reed & Campbell 1962). This suggests that the following two approaches can be used to study its motion (see Solomon (1970) for a more general discussion).

(i) In the first approach, the motion of individual ice floes is studied by solving Newton's equations for each floe taking into account any floe–floe interactions. From these solutions, one then extracts statistical information (Thorndike & Colony 1982; Colony & Thorndike 1984, 1985; Thorndike 1986; Rampal *et al.* 2009; Agarwal & Wettlaufer 2017) that is used to describe the motion of the ice cover at much larger length scales.

(ii) In the second, one takes the ice cover to be a continuum and develops rheological models to relate the internal stress field to the other macroscopic variables, including the thickness distribution of ice (Thorndike *et al.* 1975; Toppaladoddi & Wettlaufer 2015, 2017; Toppaladoddi, Moon & Wettlaufer 2023). This is then used in the Cauchy equation, with appropriate boundary conditions, to solve for the velocity field.

A principal aim of both these approaches is to predict the statistical properties of the ice velocity field. Both approaches have their advantages and limitations, but the focus since the Arctic Ice Dynamics Joint Experiment (AIDJEX) expedition in the 1970s has been on developing observationally consistent rheological models (Rothrock 1975*a*; Feltham 2008).

The first attempt to include floe–floe interactions into the dynamics of sea ice was by Sverdrup (1928). He represented the internal ice resistance using a frictional force that was proportional to the floe velocity, but always in the direction opposite to it. However, this formulation is not completely correct as friction can both decelerate and accelerate an object depending on the relative velocity (Reed & Campbell 1962; Solomon 1970). A more generalised description of the floe–floe interactions was developed by Solomon (1970) and Timokhov (1970), who considered deterministic and stochastic drift of ice, respectively, in one dimension. In a more general approach, the ice cover has been treated as a two-dimensional granular gas to understand the emergence of internal stress from floe–floe collisions (Shen, Hibler & Leppäranta 1987) and the motion of ice floes in the marginal ice zone (Feltham 2005).

In order to study the emergence of internal stress from floe–floe collisions and the fracturing of floes, detailed numerical investigations have been performed using the molecular dynamics (Herman 2011, 2013) and discrete element modelling (Hopkins 1996; Hopkins & Thorndike 2006; Herman 2016) approaches. Furthermore, new discrete element methods have been developed to: (i) simulate ice dynamics in a Lagrangian frame (Damsgaard, Adcroft & Sergienko 2018); (ii) resolve changes in the floe geometry resulting from collisions and mechanical deformation (Manucharyan & Montemuro 2022); (iii) capture dynamic sea ice patterns (West *et al.* 2022); (iv) study pressure ridging (Damsgaard, Sergienko & Adcroft 2021); and (v) understand the interactions between sea ice and ocean waves (Herman 2017). These new methods use different models to

represent floe–floe interactions, including Coulomb friction models (Damsgaard *et al.* 2018; Manucharyan & Montemuro 2022).

More recently, the $\mu(I)$ rheology – which was originally developed to model the viscoplastic flows of dense granular materials (da Cruz *et al.* 2005) – has been used to describe the flow of sea ice in the marginal ice zone. Herman (2022) and de Diego *et al.* (2024), assuming sea ice rheology to be the $\mu(I)$ rheology, have used data from their discrete element simulations to infer the friction coefficient, μ, and dilatancy, Φ, as functions of the inertial number, I, which is defined as the ratio of inertial to pressure forces (da Cruz *et al.* 2005). The dimensionless parameter I determines the state of the system which can be quasistatic ($I \leqslant 10^{-3}$) or collision dominated ($I \geqslant 10^{-1}$), with an intermediate transition regime ($10^{-3} < I < 10^{-1}$) (da Cruz *et al.* 2005).

Simulating the dynamics of individual floes using discrete element methods provides the most detailed description of the ice cover; however, this approach becomes computationally prohibitive when extended to large spatial domains (Manucharyan & Montemuro 2022). One way to circumvent this computational difficulty is through the use of a continuum description of the ice cover. The collective motion of ice floes on length scales much larger than the floe scale can be approximated as that of a continuum (Thorndike *et al.* 1975). In this case, the equations that describe the evolution of the ice cover are the mass balance and Cauchy equations (Untersteiner 1986). The principal challenge associated with this approach has been in determining the constitutive equation for the internal stress (Rothrock 1975*a*). This task is made more difficult by the fact that the stress field in the ice cover depends not just on strain and strain rate but also on ice thickness and its distribution (Untersteiner 1986). Hence, understanding the coupling between the dynamics and the state of the ice cover, which is quantified by the thickness distribution of sea ice (Thorndike *et al.* 1975; Toppaladoddi & Wettlaufer 2015), is necessary.

The internal stress field in the ice cover is a consequence of the mechanical interactions between the constituent ice floes (Evans 1970; Rothrock 1975*a*). However, unlike in the kinetic theory of gases, where molecules are assumed to interact only via elastic collisions (Harris 1971; Chapman & Cowling 1990), there are different modes of interaction – rafting, ridging, shearing and jostling – between ice floes (Parmerter & Coon 1972; Rothrock 1975*a*; Parmerter 1975; Vella & Wettlaufer 2008). This makes it more challenging to develop a Boltzmann-like theory for the velocity distribution, although the development of such a theory has been attempted in the context of Saturn's rings (Goldreich & Tremaine 1978), where the shearing and jostling modes of interaction between ice particles are possible. In addition to the above four modes, the individual ice floes can also fracture due to thermal stresses (Evans & Untersteiner 1971) and due to interactions with ocean waves (Asplin *et al.* 2012).

A feature that is common to all these modes of interaction is that they happen over time and length scales much shorter than those that characterise the geophysical-scale evolution of the ice cover (Toppaladoddi & Wettlaufer 2015). This naturally leads to the following questions which any theory of sea ice rheology must address in one form or another. (i) What contributions do these different modes of interaction make to the rheology of the ice cover? (ii) What modes of interaction are important on different time scales? (iii) How are these interactions incorporated into a continuum description of the ice cover? Indeed, we will use these questions to guide us in the development of our own theory. In the development of viscous and plastic rheological models for sea ice, considerable emphasis was placed on the connection between the floe–floe interactions and the continuum behaviour (Rothrock 1975*a*). For this reason, we present a detailed discussion of these models here.

Some of the earliest rheological models proposed to study ice dynamics were the viscous models (Reed & Campbell 1962; Campbell 1965; Rothrock 1975a). Based on their qualitative observations of sea ice motion, Reed & Campbell (1962) argued that the floe–floe interactions (shearing and jostling) should transport momentum from the faster moving to slower moving regions of the ice cover. This led them to propose a Newtonian rheology for sea ice. Subsequently, Nye (1973) and Hibler (1977) provided more detailed arguments for the viscous behaviour to be viewed as the averaged response of the ice cover over long time and large length scales. There are a few variants of the viscous model that have been suggested, but not all are physically consistent (Rothrock 1975a).

The viscous model of Rothrock (1975a,b), in combination with a divergence-free velocity field, produces realistic drift of the Arctic ice cover. However, the viscous models of sea ice, in general, suffer from the following two limitations. The first limitation is that there is no theoretical framework to estimate the values of shear and bulk viscosity coefficients; hence they can only be determined empirically (Rothrock 1975a). The second is that there is no agreement on what the correct values of the viscosity coefficients are: in previous studies, the value of shear viscosity had to be varied by three orders of magnitude to reproduce numerically the different features of the ice cover (Rothrock 1975a,b). These results suggest that the viscosity coefficients depend strongly on the state of the ice cover. However, to our knowledge, there have been no attempts at developing a more systematic theory to connect these rheological properties to the thickness distribution. A more detailed discussion of the viscous models can be found in the review by Rothrock (1975a).

The limitations of the viscous models, along with the difficulty of making stronger connections between them and the modes of floe–floe interactions, might be the key reasons why these models were abandoned and, at the same time, motivated the development of complex rheological models. During the AIDJEX project, a detailed study of the ridging/rafting processes was undertaken (Parmerter & Coon 1972; Parmerter 1975), and this led Coon *et al.* (1974) to develop the elastic–plastic rheological model. In this model, sea ice behaves like an elastic solid when the stress state lies in the interior of the yield curve, which is given by $F(\sigma_I, \sigma_{II}) = 0$, where F is the yield function and σ_I and σ_{II} are the two invariants of the two-dimensional stress tensor $\boldsymbol{\sigma}$. When the stress state lies on the yield curve, the deformation rate is given by the plastic flow rule,

$$\dot{\boldsymbol{\epsilon}}_p = \lambda \left. \frac{\partial F}{\partial \boldsymbol{\sigma}} \right|_{F=0}. \tag{1.1}$$

Here, $\dot{\boldsymbol{\epsilon}}_p$ is the plastic rate-of-strain tensor and λ is a scalar that has to be determined as a part of the solution (Coon *et al.* 1974). We note that the plastic flow rule (1.1) can be arrived at using a variational argument (Howell, Kozyreff & Ockendon 2009).

The justifications provided for the elastic–plastic model are that (Coon *et al.* 1974): (i) during ridging/rafting of ice floes the work done against gravity, assuming no energy loss to friction, appears as the potential energy of the ridged/rafted floes, with the end result being independent of the rate at which ridging/rafting proceeds; and (ii) sea ice shares visual similarity with other materials that have been successfully modelled using plastic rheologies. Furthermore, Coon *et al.* (1974) linked the yield function of the plastic response to the thickness distribution, thus coupling the rheology to the state of the ice cover. These ideas also led to the subsequent development of viscous–plastic (Hibler 1979) and elastic–viscous–plastic (Hunke & Dukowicz 1997) models, which are some of the more widely used rheological models in current climate models (Keen *et al.* 2021). This is because they are easier to implement numerically than the elastic–plastic model

(Hibler 1979; Hunke & Dukowicz 1997; Feltham 2008). More recently, anisotropic (Wilchinsky & Feltham 2004; Tsamados, Feltham & Wilchinsky 2013) and brittle (Girard *et al.* 2011; Bouillon & Rampal 2015; Dansereau *et al.* 2016; Ólason *et al.* 2022) rheological models have been developed to capture some of the observed features in pack ice.

Results from these different rheological models have been compared with observations for fluctuations in sea ice extent (Agarwal & Wettlaufer 2018), trends in sea ice drift and acceleration (Rampal *et al.* 2011) and linear kinematic features in pack ice (Bouchat *et al.* 2022; Hutter *et al.* 2022). These studies show that the rheological models reproduce the observed features with mixed degrees of success.

From this discussion of the literature, it is clear that the focus of the past studies was either on floe-scale dynamics or on the development of rheological models. Although the development of viscous and plastic rheologies were motivated by the need to understand the consequences of floe–floe interactions on the dynamics at the continuum scale, any connection between the dynamics at these extreme scales remains tenuous. To our knowledge, there have been no attempts to systematically bridge the gap between these two scales. Hence, our goal here is to obtain the rheological properties of sea ice starting from the floe-scale dynamics. We achieve this using tools from statistical physics (Harris 1971; Chapman & Cowling 1990).

We begin by first constructing a mean-field description of the stochastic motion of a single floe. Our picture of the mean-field approximation of floe–floe interactions is analogous to that of a Brownian particle subjected to dry frictional force (Elmer 1997; de Gennes 2005; Hayakawa 2005) in an external force field. The introduction of the dry (or Coulomb) friction, whose direction depends on the sign of the relative velocity of the floe with respect to the mean velocity, addresses the principal shortcoming of Sverdrup's model (Sverdrup 1928). This approach allows us to obtain a generalised Fokker–Planck equation, also called the Kramers–Chandrasekhar equation (Kramers 1940; Chandrasekhar 1943), for the probability density function (PDF) of velocity fluctuations. We then obtain the continuum equations of motion through a Chapman–Enskog analysis (Lebowitz, Frisch & Helfand 1960; Chapman & Cowling 1990) of this equation. In our case, the Newtonian rheology that emerges at large scales is a direct consequence of the dynamics at the floe scale.

The remainder of the paper is organised as follows. We begin in § 2 with the development of the stochastic model for the motion of an ice floe and obtain the kinetic equation for the PDF of its velocity. In § 3, we perform a Chapman–Enskog analysis of the kinetic equation and obtain the continuum equations of motion, including the rheological model that emerges from the floe-scale dynamics. Then, in § 4, we compare some of our results with observations and idealised large-scale simulations of ice drift, and then end with a summary of our study in § 5.

2. Stochastic drift of an ice floe

Here we consider the motion of a single floe and develop a mean field theory for its interactions with its neighbouring floes. For simplicity, we consider the ice floe to be a rigid circular disc with thickness h and radius R (see figure 1). In the region containing the floe, the ice concentration, which is defined as the fraction of the area of this region covered by ice, is $\mathcal{C}$ and the mean thickness of the ice cover is $\mathcal{H}$. Apart from these bulk quantities, we ignore all other details – such as the geometry, thickness and floe size – of the neighbouring floes.
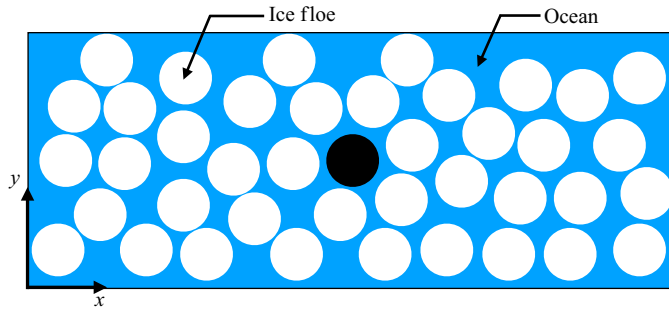
Figure 1. Schematic of the domain considered. The ice floe considered (in black) is assumed to be a circular disc with radius R and thickness h. The ice concentration and the mean thickness in the region containing this floe are taken to be $\mathcal{C}$ and $\mathcal{H}$, respectively.

2.1. *Langevin equation*

The equations governing the horizontal motion of the floe are

$$\frac{\mathrm{d}\boldsymbol{x}}{\mathrm{d}t} = \boldsymbol{v}, \tag{2.1}$$

and

$$\frac{\mathrm{d}}{\mathrm{d}t}(m\,\boldsymbol{v}) = \boldsymbol{F}_a + \mathcal{B}\,\boldsymbol{\xi}(t) - \boldsymbol{F}_o + \boldsymbol{F}_G + \boldsymbol{F}_H - 2\,m\,\Omega_0\,\boldsymbol{k}\times\boldsymbol{v} - \mathcal{F}\,\boldsymbol{S}(\boldsymbol{v}-\boldsymbol{u}^\infty). \tag{2.2}$$

Here, $\boldsymbol{x} = (x, y)$ is the position vector, $\boldsymbol{v} = (u, v)$ is its two-dimensional velocity and m is the mass of the ice floe. The wind forcing is separated into mean, $\boldsymbol{F}_a(\boldsymbol{x}, t)$, and fluctuations, $\mathcal{B}\,\boldsymbol{\xi}(t)$, with $\mathcal{B}$ being the amplitude of the fluctuations and $\boldsymbol{\xi}(t)$ being Gaussian white noise. The ocean drag force is represented by $\boldsymbol{F}_o(\boldsymbol{x}, t)$, which subsumes the contributions from skin friction and form drag (Steele, Morison & Untersteiner 1989). Forces due to gradients in the atmospheric pressure and sea surface height are represented by $\boldsymbol{F}_G(\boldsymbol{x}, t)$ and $\boldsymbol{F}_H(\boldsymbol{x}, t)$, respectively. The fourth term on the right-hand side of (2.2) represents the Coriolis force with Ω_0 being the Coriolis frequency and $\boldsymbol{k}$ the unit vector along the vertical. The last term represents the force on the floe that results from its interactions with the neighbouring floes. We model this force using Coulomb's dry friction model (Elmer 1997); $\mathcal{F} \equiv \mathcal{F}[g(\boldsymbol{x}, h, t)]$ represents the magnitude of the frictional force, $g(\boldsymbol{x}, h, t)$ is the sea ice thickness distribution, and $\boldsymbol{S}$ is a unit vector given by

$$\boldsymbol{S}(\boldsymbol{v}-\boldsymbol{u}^\infty) = \frac{\boldsymbol{v}-\boldsymbol{u}^\infty}{|\boldsymbol{v}-\boldsymbol{u}^\infty|}, \tag{2.3}$$

where $\boldsymbol{u}^\infty$ is the mean velocity. The function $\boldsymbol{S}$ is a generalisation of the sign function for a two-dimensional vector. Introducing the fluctuating velocity as $\boldsymbol{v}' = \boldsymbol{v} - \boldsymbol{u}^\infty$, we write (2.3) as

$$\boldsymbol{S}(\boldsymbol{v}') = \frac{\boldsymbol{v}'}{|\boldsymbol{v}'|}. \tag{2.4}$$

Here, we ignore any rotational motion of the floe caused by floe–floe interactions. The magnitude $\mathcal{F}$ represents the minimum force required to set the floe into motion starting from rest, and hence represents the threshold value of the frictional force. To establish the dependence of $\mathcal{F}$ on $g(\boldsymbol{x}, h, t)$, we follow Hibler (1979) and use the first two moments of
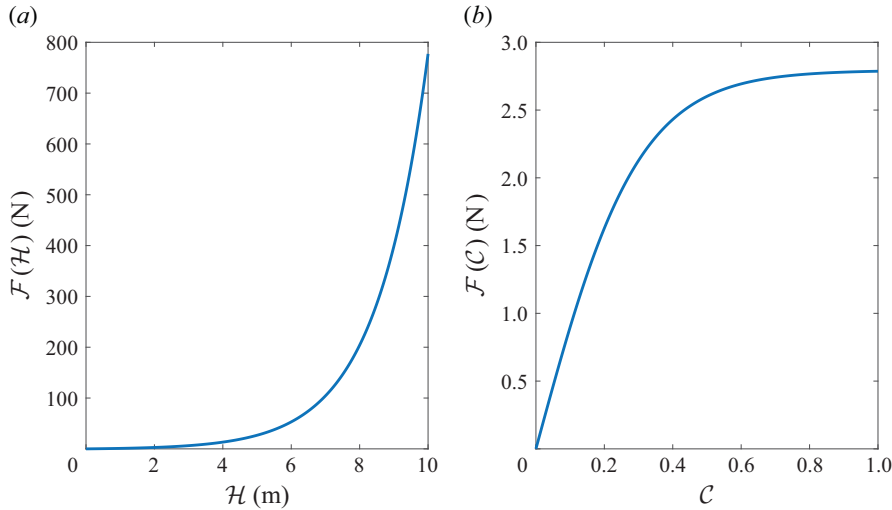
1014 A6-6

Figure 2. The qualitative behaviour of the threshold force $\mathcal{F}$ with varying values of (*a*) mean thickness ($\mathcal{H}$) and (*b*) concentration ($\mathcal{C}$). In (*a*) the value of $\mathcal{C}$ is fixed to 0.8, and in (*b*) the value of $\mathcal{H}$ is fixed to 2 m. The values of the other parameters are $\mathcal{F}_0 = 1$ N, $\mathcal{H}_0 = 1.5$ m and $\mathcal{C}_0 = 0.3$.

$g(\boldsymbol{x}, h, t)$, which are $\mathcal{C}$ and $\mathcal{H}$. In terms of $g(\boldsymbol{x}, h, t)$, these are given by (Toppaladoddi *et al.* 2023)

$$\mathcal{C}(\boldsymbol{x}, t) = \int_{0^+}^{\infty} g(\boldsymbol{x}, h, t)\, \mathrm{d}h, \tag{2.5}$$

and

$$\mathcal{H}(\boldsymbol{x}, t) = \int_{0^+}^{\infty} h\, g(\boldsymbol{x}, h, t)\, \mathrm{d}h. \tag{2.6}$$

The dependence of $\mathcal{F}$ on $\mathcal{C}$ and $\mathcal{H}$ is determined by considering the following:

(i) in the limits $\mathcal{C} \to 0$ and/or $\mathcal{H} \to 0$ the interaction term should vanish as the ice cover vanishes;
(ii) as $\mathcal{C} \to 1$, the threshold force $\mathcal{F}$ becomes independent of $\mathcal{C}$ as the number of ice floes that could interact with the chosen floe saturates;
(iii) $\mathcal{F}$ should increase with increasing $\mathcal{H}$ as the resistance offered by the neighbouring floes increases.

A functional form of $\mathcal{F}$ that satisfies these constraints is

$$\mathcal{F}(\mathcal{C}, \mathcal{H}) = \mathcal{F}_0 \left[\exp\left(\frac{\mathcal{H}}{\mathcal{H}_0}\right) - 1 \right] \tanh\left(\frac{\mathcal{C}}{\mathcal{C}_0}\right). \tag{2.7}$$

Here, $\mathcal{F}_0$ depends on ice strength and the amplitude of wind forcing, but for simplicity we assume it to be a constant; $\mathcal{H}_0$ is the equilibrium thickness which from observations is 1.5 m (Toppaladoddi & Wettlaufer 2015) and the value $\mathcal{C}_0 = 0.3$ is chosen such that $\tanh(\mathcal{C}/\mathcal{C}_0) = 1$ for $\mathcal{C} \geqslant 0.8$. Figure 2 shows the qualitative behaviour of $\mathcal{F}$ with varying values of $\mathcal{H}$ and $\mathcal{C}$. We should emphasise here that this functional form is not unique.

In introducing the floe–floe interaction term in (2.2), we have made the following assumptions: (i) (inelastic) collisions that involve only jostling and/or shearing between ice floes are important, and (ii) the role of collisions here is to drive the velocity to its

mean value, $\boldsymbol{u}^\infty$. On shorter time scales the motion of the ice floes is determined by wind forcing (Thorndike & Colony 1982), which results in the different modes of interaction between ice floes discussed in § 1. Assumptions (i) and (ii) imply that only the shearing and jostling modes drive the system towards local equilibrium and the other two modes (rafting and ridging) do not. Hence, the rheology of the ice cover for large time and length scales will be determined by the shearing and jostling modes.

Our model can be justified using the following arguments. If $N(\gg 1)$ is the total number of floes, then any description of a single floe requires us to take into account its interactions with its $n(\ll N)$ nearest neighbours. However, the construction of a system of coupled deterministic/stochastic differential equations for these localised interactions would also require us to take into account the interactions of the neighbouring floes with their own nearest neighbours. Hence, any description of the dynamics of a subset of the N floes leads to a closure problem, which is similar to the closure problem encountered in the kinetic theory of gases (Grad 1958; Harris 1971). Consequently, some assumptions would have to be made to truncate the problem. The mathematical form of the interactions in (2.2) represents a mean-field approximation of these interactions. This term embodies the fact that the collisions between the floe and its neighbours are due to the different velocities with which they move. However, if they all were to move with the mean velocity $\boldsymbol{u}^\infty$ then they would not collide with each other, in which case $\boldsymbol{S} = \boldsymbol{0}$. It is important to highlight that the mathematical representation of the floe–floe interactions in (2.2) permits both acceleration and deceleration of the ice floe depending on the sign of the fluctuation.

Assuming m to be a constant, which implies the absence of thermal growth and ridging and rafting of ice floes, (2.2) becomes

$$\frac{\mathrm{d}\boldsymbol{v}}{\mathrm{d}t} = \frac{1}{m}\,\boldsymbol{F}^{ext} - f\,\boldsymbol{S}(\boldsymbol{v}') + b\,\boldsymbol{\xi}(t), \tag{2.8}$$

where $\boldsymbol{F}^{ext} = \boldsymbol{F}_a - \boldsymbol{F}_o + \boldsymbol{F}_G + \boldsymbol{F}_H - 2\,m\,\Omega_0\,\boldsymbol{k}\times\boldsymbol{v}$, $b = \mathcal{B}/m$ and $f = \mathcal{F}/m$. We are interested in the statistical properties of $\boldsymbol{v}$; but, unlike for the Langevin equation for the classical Brownian motion problem (Uhlenbeck & Ornstein 1930; Reif 1965), it is difficult to solve (2.8) to obtain the moments of $\boldsymbol{v}$ because of the nonlinear function $\boldsymbol{S}$. For this reason, and for developing a continuum theory, we consider the PDF of $\boldsymbol{v}$.

2.2. *The Kramers-Chandrasekhar Equation (KCE)*

The generalised Fokker–Planck equation or the KCE for the PDF, $\tilde{P}(\boldsymbol{x}, \boldsymbol{v}, t)$, corresponding to (2.8) is

$$\frac{\partial \tilde{P}}{\partial t} + \boldsymbol{v}\cdot\nabla_{\boldsymbol{x}}\tilde{P} + \frac{\boldsymbol{F}^{ext}}{m}\cdot\nabla_{\boldsymbol{v}}\tilde{P} = \nabla_{\boldsymbol{v}}\cdot\{[f\,\boldsymbol{S}(\boldsymbol{v}')]\,\tilde{P} + D\,\nabla_{\boldsymbol{v}}\tilde{P}\}. \tag{2.9}$$

Here, $\tilde{P}(\boldsymbol{x}, \boldsymbol{v}, t)\,\mathrm{d}\boldsymbol{x}\,\mathrm{d}\boldsymbol{v}$ represents the probability that the floe's velocity lies in the range $(\boldsymbol{v}, \boldsymbol{v} + \mathrm{d}\boldsymbol{v})$ and in a region $(\boldsymbol{x}, \boldsymbol{x} + \mathrm{d}\boldsymbol{x})$ at time t, $\nabla_{\boldsymbol{x}}$ and $\nabla_{\boldsymbol{v}}$ are the gradient operators in physical and velocity spaces, respectively, and $D = b^2/2$ is the diffusion coefficient for diffusion of $\tilde{P}$ in velocity space. The procedure for obtaining (2.10) using (2.8) is a standard one and is found elsewhere (Chandrasekhar 1943; Doering 2018). We now introduce $\mathcal{P} = m\,N\,\tilde{P}$, with N being the total constant number of floes, such that $\mathcal{P}\,\mathrm{d}\boldsymbol{x}\,\mathrm{d}\boldsymbol{v}$ gives the mass in the phase-space volume element $\mathrm{d}\boldsymbol{x}\,\mathrm{d}\boldsymbol{v}$. To obtain the evolution equation for $\mathcal{P}$ we multiply (2.9) with $m\,N$, which gives

$$\frac{\partial \mathcal{P}}{\partial t} + \boldsymbol{v}\cdot\nabla_{\boldsymbol{x}}\mathcal{P} + \frac{\boldsymbol{F}^{ext}}{m}\cdot\nabla_{\boldsymbol{v}}\mathcal{P} = \nabla_{\boldsymbol{v}}\cdot\{[f\,\boldsymbol{S}(\boldsymbol{v}')]\,\mathcal{P} + D\,\nabla_{\boldsymbol{v}}\mathcal{P}\}. \tag{2.10}$$

Assuming the correlation time scale associated with the velocity fluctuations of the floe to be smaller than Ω_0^{-1}, we can neglect the Coriolis effect on the velocity fluctuations. This then leads to these fluctuations being isotropic. (We will test the veracity of this assumption by comparing our results with observations.) In addition, although the Coriolis force influences the route to equilibrium, the equilibrium solution itself should be independent of it. This is because the Coriolis force does not contribute to the relaxation of the system like the floe–floe collisions do. The Coriolis effect here is qualitatively similar to the effect of a weak magnetic field acting on a charged Brownian particle; the equilibrium PDF in this case is independent of the magnetic field (Wycoff & Balazs 1987). Hence, following Maxwell (1860), we conclude that the equilibrium PDF should be an even function of $(\boldsymbol{v} - \boldsymbol{u}^\infty)$. However, contrary to Maxwell's assumption (Maxwell 1860), the fluctuations in u and v are not independent because of the coupling through $\boldsymbol{S}(\boldsymbol{v}')$.

The macroscopic variables are now obtained as moments of $\mathcal{P}$ (Harris 1971; Chapman & Cowling 1990):

(i) mass density,

$$\rho(\boldsymbol{x}, t) = \int \mathcal{P}(\boldsymbol{x}, \boldsymbol{v}, t) \, \mathrm{d}\boldsymbol{v}; \tag{2.11}$$

(ii) momentum density,

$$\rho(\boldsymbol{x}, t) \, \boldsymbol{u}^\infty(\boldsymbol{x}, t) = \int \boldsymbol{v} \, \mathcal{P}(\boldsymbol{x}, \boldsymbol{v}, t) \, \mathrm{d}\boldsymbol{v}; \tag{2.12}$$

(iii) energy density,

$$\rho(\boldsymbol{x}, t) \, \mathcal{E}(\boldsymbol{x}, t) = \tfrac{1}{2} \int \left(\boldsymbol{v} - \boldsymbol{u}^\infty\right)^2 \mathcal{P}(\boldsymbol{x}, \boldsymbol{v}, t) \, \mathrm{d}\boldsymbol{v}. \tag{2.13}$$

Here, ρ denotes the mass density per unit area in the chosen region; it is, however, not related to the mass density of the ice floe itself, which has the units of mass per unit volume. In the case of a dilute gas, the kinetic energy associated with the velocity fluctuations (2.13), in/close to equilibrium, is related to the temperature of the gas (Harris 1971; Chapman & Cowling 1990; Lifshitz & Pitaevskii 2005). In our case, however, the velocity fluctuations do not have any thermodynamic significance.

3. The continuum theory

3.1. *The macroscopic equations*

As the macroscopic variables are obtained as moments of $\mathcal{P}$ ((2.11)–(2.13)), the equations that govern their spatiotemporal evolution are obtained as appropriate moments of (2.10). To simplify the analysis, we make a change of variables from $(\boldsymbol{x}_o, \boldsymbol{v}, t_o)$ to $(\boldsymbol{x}_n, \boldsymbol{v}', t_n)$, where the subscripts 'o' and 'n' stand for old and new. Using $\boldsymbol{v} = \boldsymbol{u}^\infty + \boldsymbol{v}'$, we obtain the transformed differential operators as (Chapman & Cowling 1990):

(i) time derivative,

$$\frac{\partial}{\partial t_o} = \frac{\partial}{\partial t_n} - \frac{\partial \boldsymbol{u}^\infty}{\partial t_n} \cdot \frac{\partial}{\partial \boldsymbol{v}'}; \tag{3.1}$$

(ii) spatial gradient operator,

$$\frac{\partial}{\partial \boldsymbol{x}_o} = \frac{\partial}{\partial \boldsymbol{x}_n} - \frac{\partial \boldsymbol{u}^\infty}{\partial \boldsymbol{x}_n} \cdot \frac{\partial}{\partial \boldsymbol{v}'}; \tag{3.2}$$

(iii) velocity gradient operator,

$$\frac{\partial}{\partial \boldsymbol{v}} = \frac{\partial}{\partial \boldsymbol{v}'}. \tag{3.3}$$

Hence, the transformed KCE is

$$\frac{\partial \mathcal{P}}{\partial t} + (\boldsymbol{u}^\infty + \boldsymbol{v}') \cdot \nabla_{\boldsymbol{x}} \mathcal{P} + \frac{\boldsymbol{F}^{ext}}{m} \cdot \nabla_{\boldsymbol{v}'} \mathcal{P} - \boldsymbol{v}' \cdot \left(\nabla_{\boldsymbol{x}} \boldsymbol{u}^\infty \cdot \nabla_{\boldsymbol{v}'} \mathcal{P} \right)$$

$$= \nabla_{\boldsymbol{v}'} \cdot \{ [f\, \boldsymbol{S}(\boldsymbol{v}')]\, \mathcal{P} + D\, \nabla_{\boldsymbol{v}'} \mathcal{P} \}, \tag{3.4}$$

where the subscript 'n' has been dropped. The following macroscopic equations are obtained by multiplying (3.4) by 1, $\boldsymbol{v}'$ and $v'^2/2$ and integrating with respect to $\boldsymbol{v}'$:

(i) mass balance equation,

$$\frac{\partial \rho}{\partial t} + \nabla_{\boldsymbol{x}} \cdot (\rho\, \boldsymbol{u}^\infty) = 0; \tag{3.5}$$

(ii) momentum balance equation,

$$\frac{\mathcal{D} \boldsymbol{u}^\infty}{\mathcal{D}t} = \frac{1}{m}\ (\boldsymbol{F}_a - \boldsymbol{F}_o + \boldsymbol{F}_G + \boldsymbol{F}_H) - 2\, \Omega_0\, \boldsymbol{k} \times \boldsymbol{u}^\infty + \frac{1}{\rho} \nabla_{\boldsymbol{x}} \cdot \boldsymbol{\sigma}, \tag{3.6}$$

where

$$\frac{\mathcal{D}}{\mathcal{D}t} = \frac{\partial}{\partial t} + \boldsymbol{u}^\infty \cdot \nabla_{\boldsymbol{x}} \tag{3.7}$$

is the total derivative, and the stress tensor, $\boldsymbol{\sigma}$, is given by

$$\boldsymbol{\sigma}(\boldsymbol{x}, t) = -\int\ \boldsymbol{v}'\, \boldsymbol{v}'\, \mathcal{P}(\boldsymbol{x}, \boldsymbol{v}', t)\, \mathrm{d}\boldsymbol{v}', \tag{3.8}$$

which has the units of force per unit length;

(iii) energy balance equation,

$$\frac{\mathcal{D}}{\mathcal{D}t} (\rho\, \mathcal{E}) + \rho\, \mathcal{E}\, \nabla_{\boldsymbol{x}} \cdot \boldsymbol{u}^\infty = -\nabla_{\boldsymbol{x}} \cdot \boldsymbol{\mathcal{Q}} - \boldsymbol{\sigma} : \nabla_{\boldsymbol{x}} \boldsymbol{u}^\infty + 2\left(D - f\int |\boldsymbol{v}'|\, \mathcal{P}\, \mathrm{d}\boldsymbol{v}' \right), \tag{3.9}$$

where $|\boldsymbol{v}'|$ is the magnitude of $\boldsymbol{v}'$, and

$$\boldsymbol{\mathcal{Q}}(\boldsymbol{x}, t) = \tfrac{1}{2} \int \boldsymbol{v}'\, v'^2\, \mathcal{P}(\boldsymbol{x}, \boldsymbol{v}', t)\, \mathrm{d}\boldsymbol{v}' \tag{3.10}$$

is the 'heat flux' vector.

Except for the last term in (3.9), these equations are similar to the ones that have been obtained for a dilute gas (Harris 1971; Chapman & Cowling 1990) and for non-interacting classical Brownian particles (Lebowitz *et al.* 1960; de Groot & Mazur 2013). This term represents the difference between the energy input from the wind forcing and the frictional loss due to the inelastic collisions between the floe and its neighbours. Energy balance can

be achieved by demanding that these two terms balance, but this would imply that the amplitude of fluctuations in wind forcing changes with the state of the ice cover. This is clearly unphysical; hence, these two terms in principle do not balance. Due to the lack of any thermodynamic significance of the velocity fluctuations, we shall not consider the energy balance equation any further.

To complete the momentum balance equation we have to evaluate the integral in (3.8) to determine $\boldsymbol{\sigma}$, and to do this we need to solve the KCE (2.10).

3.2. *Chapman–Enskog analysis*

In order to obtain solutions to (2.10) using the Chapman–Enskog method (Lebowitz *et al.* 1960; Lifshitz & Pitaevskii 2005; de Groot & Mazur 2013), we first make the equation dimensionless by choosing R as the length scale, Ω_0^{-1} as the time scale, $R\,\Omega_0$ as the velocity scale and $m/(\Omega_0^2\,R^4)$ as the scale for $\mathcal{P}$. Using these, we get the dimensionless KCE to be

$$\frac{\partial \mathcal{P}_d}{\partial t_d} + \boldsymbol{v}_d \cdot \nabla_{\boldsymbol{x}_d} \mathcal{P}_d + \boldsymbol{F}_d^{ext} \cdot \nabla_{\boldsymbol{v}_d} \mathcal{P}_d = \frac{1}{\epsilon}\,\nabla_{\boldsymbol{v}_d} \cdot \left\{ \mathcal{M}\,\boldsymbol{S}(\boldsymbol{v}_d')\,\mathcal{P}_d + \nabla_{\boldsymbol{v}_d}\mathcal{P}_d \right\}, \qquad (3.11)$$

where the subscript d denotes a dimensionless variable, $\epsilon = \Omega_0^3\,R^2/D$, and $\mathcal{M} = (f\,R\,\Omega_0)/D$ is the dimensionless threshold force. As $\Omega_0 \sim 10^{-4}$ s^{-1}, $R \sim 10^3$ m and $D \sim 1$ m^2 s^{-3}, we have $\epsilon \ll 1$. Using this small parameter we now expand $\mathcal{P}_d$ in a perturbative series

$$\mathcal{P}_d = \mathcal{P}_d^{(0)} + \epsilon\,\mathcal{P}_d^{(1)} + \epsilon^2\,\mathcal{P}_d^{(2)} + \dots, \qquad (3.12)$$

where $\mathcal{P}_d^{(0)}$ is the local equilibrium distribution. We demand that

$$\int \mathcal{P}_d^{(0)} \begin{bmatrix} 1 \\ \boldsymbol{v}_d \\ \dfrac{\left(\boldsymbol{v}_d - \boldsymbol{u}_d^\infty\right)^2}{2} \end{bmatrix} \mathrm{d}\boldsymbol{v} = \begin{bmatrix} \rho_d \\ \rho_d\,\boldsymbol{u}_d^\infty \\ \rho_d\,\mathcal{E} \end{bmatrix}, \qquad (3.13)$$

and that the deviations from the local equilibrium distribution do not contribute to the macroscopic variables, i.e.

$$\int \mathcal{P}_d^{(i)} \begin{bmatrix} 1 \\ \boldsymbol{v}_d \\ \dfrac{\left(\boldsymbol{v}_d - \boldsymbol{u}_d^\infty\right)^2}{2} \end{bmatrix} \mathrm{d}\boldsymbol{v} = \begin{bmatrix} 0 \\ 0 \\ 0 \end{bmatrix}; \quad i = 1, 2, 3, \dots. \qquad (3.14)$$

Using the expansion in (3.11) we get

$$\epsilon\left[\frac{\partial \mathcal{P}_d^{(0)}}{\partial t_d} + \boldsymbol{v}_d \cdot \nabla_{\boldsymbol{x}_d}\mathcal{P}_d^{(0)} + \boldsymbol{F}_d^{ext} \cdot \nabla_{\boldsymbol{v}_d}\mathcal{P}_d^{(0)}\right] = \left[\nabla_{\boldsymbol{v}_d} \cdot \left\{\mathcal{M}\,\boldsymbol{S}(\boldsymbol{v}_d')\,\mathcal{P}_d^{(0)} + \nabla_{\boldsymbol{v}_d}\mathcal{P}_d^{(0)}\right\}\right]$$

$$+ \epsilon\left[\nabla_{\boldsymbol{v}_d} \cdot \left\{\mathcal{M}\,\boldsymbol{S}(\boldsymbol{v}_d')\,\mathcal{P}_d^{(1)} + \nabla_{\boldsymbol{v}_d}\mathcal{P}_d^{(1)}\right\}\right]$$

$$+ O(\epsilon^2).$$

$$(3.15)$$

3.2.1. *Calculation of $\mathcal{P}_d^{(0)}$*

Collecting terms of $O(1)$ gives

$$\nabla_{\boldsymbol{v}_d} \cdot \left[\mathcal{M} \, \boldsymbol{S}(\boldsymbol{v}_d') \, \mathcal{P}_d^{(0)} + \nabla_{\boldsymbol{v}_d} \mathcal{P}_d^{(0)} \right] = 0. \tag{3.16}$$

To solve this equation, we introduce the drift vector $\mathcal{L}$, which is defined as

$$\mathcal{L} \equiv \mathcal{M} \, \boldsymbol{S}(\boldsymbol{v}_d') = \mathcal{M} \, \frac{\boldsymbol{v}_d'}{|\boldsymbol{v}_d'|}. \tag{3.17}$$

In component form, this is written as

$$(\mathcal{L}_{u'}, \mathcal{L}_{v'}) = \left(\mathcal{M} \, \frac{u_d'}{\sqrt{u_d'^2 + v_d'^2}}, \, \mathcal{M} \, \frac{v_d'}{\sqrt{u_d'^2 + v_d'^2}} \right). \tag{3.18}$$

Using $\nabla_{\boldsymbol{v}_d} = \nabla_{\boldsymbol{v}_d'}$ it is easily seen from (3.18) that

$$\frac{\partial \mathcal{L}_{u'}}{\partial v_d'} = \frac{\partial \mathcal{L}_{v'}}{\partial u_d'} = -\mathcal{M} \, \frac{u_d' \, v_d'}{\left(u_d'^2 + v_d'^2 \right)^{3/2}}, \tag{3.19}$$

which implies that $\mathcal{L}$ can be expressed as the gradient of a potential, i.e. $\mathcal{L} = \nabla_{\boldsymbol{v}_d'} \Phi$, and that the total probability flux vanishes everywhere (Risken 1996). The required solution is readily found to be

$$\mathcal{P}_d^{(0)}(u_d', v_d') = \mathcal{N} \, \exp(-\Phi). \tag{3.20}$$

The integration constant $\mathcal{N}$ is determined by requiring that

$$\int \mathcal{P}_d^{(0)} \, \mathrm{d}\boldsymbol{v}_d' = \rho_d, \tag{3.21}$$

where $\rho_d = \rho/(m/R^2)$ is the dimensionless mass density, and

$$\Phi = \int \mathcal{L}_{u'} \, \mathrm{d}u_d' + \int \mathcal{L}_{v'} \, \mathrm{d}v_d'. \tag{3.22}$$

Using (3.18) to evaluate the integrals, we get

$$\Phi = 2 \, \mathcal{M} \, \sqrt{u_d'^2 + v_d'^2}, \tag{3.23}$$

which gives

$$\mathcal{P}_d^{(0)}(\boldsymbol{v}_d') = \frac{2 \, \rho_d \, \mathcal{M}^2}{\pi} \, \exp\left(-2 \, \mathcal{M} \, |\boldsymbol{v}_d'| \right). \tag{3.24}$$

The solution $\mathcal{P}_d^{(0)}$ represents the generalised Laplace distribution.

3.2.2. *Calculation of $\mathcal{P}_d^{(1)}$*

Next, at $O(\epsilon)$ we have

$$\nabla_{\boldsymbol{v}_d} \cdot \left\{ \mathcal{M} \, \boldsymbol{S}(\boldsymbol{v}_d') \, \mathcal{P}_d^{(1)} + \nabla_{\boldsymbol{v}_d} \mathcal{P}_d^{(1)} \right\} = \frac{\partial \mathcal{P}_d^{(0)}}{\partial t_d} + \boldsymbol{v}_d \cdot \nabla_{\boldsymbol{x}_d} \mathcal{P}_d^{(0)} + \boldsymbol{F}_d^{ext} \cdot \nabla_{\boldsymbol{v}_d} \mathcal{P}_d^{(0)}. \tag{3.25}$$

Using the solution (3.24) we evaluate the right-hand side of (3.25). To determine the time and spatial derivatives we note that the dependence of $\mathcal{P}_d^{(0)}$ on t and $\boldsymbol{x}$ is through the

1014 A6-12

macroscopic variables. Hence, we get

$$\frac{\partial \mathcal{P}_d^{(0)}}{\partial t_d} = \frac{\partial \mathcal{P}_d^{(0)}}{\partial \rho_d} \frac{\partial \rho_d}{\partial t_d} + \frac{\partial \mathcal{P}_d^{(0)}}{\partial \boldsymbol{u}_d^{\infty}} \cdot \frac{\partial \boldsymbol{u}_d^{\infty}}{\partial t_d} + \frac{\partial \mathcal{P}_d^{(0)}}{\partial \mathcal{C}} \frac{\partial \mathcal{C}}{\partial t_d} + \frac{\partial \mathcal{P}_d^{(0)}}{\partial \mathcal{H}_d} \frac{\partial \mathcal{H}_d}{\partial t_d}, \tag{3.26}$$

and

$$\frac{\partial \mathcal{P}_d^{(0)}}{\partial \boldsymbol{x}_d} = \frac{\partial \mathcal{P}_d^{(0)}}{\partial \rho_d} \frac{\partial \rho_d}{\partial \boldsymbol{x}_d} + \frac{\partial \mathcal{P}_d^{(0)}}{\partial \boldsymbol{u}_d^{\infty}} \cdot \frac{\partial \boldsymbol{u}_d^{\infty}}{\partial \boldsymbol{x}_d} + \frac{\partial \mathcal{P}_d^{(0)}}{\partial \mathcal{C}} \frac{\partial \mathcal{C}}{\partial \boldsymbol{x}_d} + \frac{\partial \mathcal{P}_d^{(0)}}{\partial \mathcal{H}_d} \frac{\partial \mathcal{H}_d}{\partial \boldsymbol{x}_d}. \tag{3.27}$$

In the absence of thermal growth and ridging and rafting, the evolution equations for $\mathcal{C}$ and $\mathcal{H}_d$, where $\mathcal{H}_d = \mathcal{H}/R$, are given by (cf. Hibler 1979)

$$\frac{\partial \mathcal{C}}{\partial t_d} + \boldsymbol{v}_d \cdot \nabla_{\boldsymbol{x}_d} \mathcal{C} = 0, \tag{3.28}$$

and

$$\frac{\partial \mathcal{H}_d}{\partial t_d} + \boldsymbol{v}_d \cdot \nabla_{\boldsymbol{x}_d} \mathcal{H}_d = 0. \tag{3.29}$$

Using (3.5), (3.6), (3.28) and (3.29) to eliminate the time derivatives in (3.26) and combining all the terms on the right-hand side of (3.25) gives

$$\text{right-hand side} = \left[-\nabla_{\boldsymbol{x}_d} \cdot \boldsymbol{u}_d^{\infty} + \frac{2 \mathcal{M}}{|\boldsymbol{v}_d'|} \boldsymbol{v}_d' \boldsymbol{v}_d' : \nabla_{\boldsymbol{x}_d} \boldsymbol{u}_d^{\infty} \right] \mathcal{P}_d^{(0)}. \tag{3.30}$$

In writing (3.30) we have omitted all terms that are linear in $\boldsymbol{v}_d'$ because

$$\int \boldsymbol{v}_d' \mathcal{P}_d^{(0)} \, \mathrm{d}\boldsymbol{v}_d' = 0. \tag{3.31}$$

Equation (3.30) suggests the functional form $\mathcal{P}_d^{(1)} = \mathcal{G} \mathcal{P}_d^{(0)}$ (Lebowitz *et al.* 1960; Lifshitz & Pitaevskii 2005), with

$$\mathcal{G} = a \left(\boldsymbol{v}_d' \boldsymbol{v}_d' - \tfrac{1}{2} v_d'^2 \, \boldsymbol{\delta} \right) : \nabla_{\boldsymbol{x}_d} \boldsymbol{u}_d^{\infty}. \tag{3.32}$$

Here, a is a constant and $\boldsymbol{\delta}$ is the Kronecker delta. This form of $\mathcal{P}_d^{(1)}$ also satisfies the constraints imposed in (3.14) (Lifshitz & Pitaevskii 2005). Using this in the left-hand side of (3.25) gives

$$\text{left-hand side} = \nabla_{\boldsymbol{v}_d} \cdot \left[\mathcal{P}_d^{(0)} \nabla_{\boldsymbol{v}_d} \mathcal{G} \right]. \tag{3.33}$$

Evaluating the expression (3.33) and comparing it with (3.30), along with the observationally consistent (Agarwal & Wettlaufer 2017) assumption that $\nabla_{\boldsymbol{x}_d} \cdot \boldsymbol{u}_d^{\infty} \approx 0$, gives $a = -1/2$. Hence, the required solution is

$$\mathcal{P}_d^{(1)} = -\frac{1}{2} \left[\left(\boldsymbol{v}_d' \boldsymbol{v}_d' - \frac{1}{2} v_d'^2 \, \boldsymbol{\delta} \right) : \nabla_{\boldsymbol{x}_d} \boldsymbol{u}_d^{\infty} \right] \mathcal{P}_d^{(0)}. \tag{3.34}$$

3.3. *The stress tensor*

Now, in order to determine the stress tensor we revert to the dimensional forms of (3.24) and (3.34), as this makes it easier to obtain the rheological properties in dimensional form.

These expressions are

$$\mathcal{P}^{(0)}(\boldsymbol{x}, \boldsymbol{v}', t) = \frac{\rho(\boldsymbol{x}, t)\, \Lambda^2}{2\,\pi}\, \exp\left(-\Lambda\,|\boldsymbol{v}'|\right), \tag{3.35}$$

with $\Lambda = 2\,f/D$, and

$$\mathcal{P}^{(1)}(\boldsymbol{x}, \boldsymbol{v}', t) = -\frac{1}{2\,D}\left[\left(\boldsymbol{v}'\boldsymbol{v}' - \frac{1}{2}\,v'^2\,\boldsymbol{\delta}\right) : \nabla_{\boldsymbol{x}}\boldsymbol{u}^\infty\right]\mathcal{P}^{(0)}(\boldsymbol{x}, \boldsymbol{v}', t). \tag{3.36}$$

Using (3.8), we have (in index notation)

$$\sigma_{ik}^{(0)} = -\int v'_i\, v'_k\, \mathcal{P}^{(0)}\, \mathrm{d}\boldsymbol{v}' = -\int v'^2\, \mathcal{P}^{(0)}\, \mathrm{d}\boldsymbol{v}'\, \delta_{ik}, \tag{3.37}$$

which gives

$$\sigma_{ik}^{(0)} = -\frac{3\,\rho}{2}\, \frac{D^2}{f_0^2}\left[\exp\left(\frac{\mathcal{H}}{\mathcal{H}_0}\right) - 1\right]^{-2}\, \coth^2\left(\frac{\mathcal{C}}{\mathcal{C}_0}\right)\, \delta_{ik}, \tag{3.38}$$

where $f_0 = \mathcal{F}_0/m$. This is the isotropic part of the stress tensor. We rewrite this expression as

$$\sigma_{ik}^{(0)} = -\Pi\, \delta_{ik}, \tag{3.39}$$

where

$$\Pi = \frac{3\,\rho}{2}\, \frac{D^2}{f_0^2}\left[\exp\left(\frac{\mathcal{H}}{\mathcal{H}_0}\right) - 1\right]^{-2}\, \coth^2\left(\frac{\mathcal{C}}{\mathcal{C}_0}\right) \tag{3.40}$$

is the pressure. Clearly, we have $\Pi \geqslant 0$.

The deviatoric part of the stress tensor is given by

$$\sigma_{ik}^{(1)} = -\int v'_i\, v'_k\, \mathcal{P}^{(1)}\, \mathrm{d}\boldsymbol{v}' = \frac{1}{2\,D}\, \frac{\partial u_m^\infty}{\partial x_n}\int v'_i\, v'_k\left[v'_m\, v'_n - \frac{1}{2}\, v'^2\, \delta_{mn}\right]\mathcal{P}^{(0)}\, \mathrm{d}\boldsymbol{v}'. \tag{3.41}$$

Assuming sea ice to be an isotropic material, the integral in the above equation can be expressed in terms of only Kronecker deltas. The combination that on contraction with indices m and n gives zero is (Lifshitz & Pitaevskii 2005)

$$\int v'_i\, v'_k\left[v'_m\, v'_n - \frac{1}{2}\, v'^2\, \delta_{mn}\right]\mathcal{P}^{(0)}\, \mathrm{d}\boldsymbol{v}' = \mathcal{A}\,\left(\delta_{im}\, \delta_{kn} + \delta_{in}\, \delta_{km} - \delta_{ik}\, \delta_{mn}\right). \tag{3.42}$$

The value of $\mathcal{A}$ is found by contracting indices i and m and k and n (Lifshitz & Pitaevskii 2005), which gives

$$\mathcal{A} = \frac{1}{8}\int v'^4\, \mathcal{P}^{(0)}\, \mathrm{d}\boldsymbol{v}'. \tag{3.43}$$

Hence,

$$\sigma_{ik}^{(1)} = \frac{1}{16\,D}\, \frac{\partial u_m^\infty}{\partial x_n}\,\left(\delta_{im}\, \delta_{kn} + \delta_{in}\, \delta_{km} - \delta_{ik}\, \delta_{mn}\right)\int v'^4\, \mathcal{P}^{(0)}\, \mathrm{d}\boldsymbol{v}'. \tag{3.44}$$

Evaluating the integral finally leads to

$$\sigma_{ik}^{(1)} = \rho\, \frac{15\, D^3}{32\, f_0^4}\left[\exp\left(\frac{\mathcal{H}}{\mathcal{H}_0}\right) - 1\right]^{-4}\, \coth^4\left(\frac{\mathcal{C}}{\mathcal{C}_0}\right)\left(\frac{\partial u_i^\infty}{\partial x_k} + \frac{\partial u_k^\infty}{\partial x_i}\right), \tag{3.45}$$

where we have used $\nabla_{\boldsymbol{x}} \cdot \boldsymbol{u}^\infty \approx 0$.

1014 A6-14

The above equation can be written as

$$\sigma_{ik}^{(1)} = \eta \, \dot{\gamma}_{ik}, \tag{3.46}$$

where

$$\eta = \rho \, \frac{15 \, D^3}{16 \, f_0^4} \left[\exp\left(\frac{\mathcal{H}}{\mathcal{H}_0}\right) - 1 \right]^{-4} \coth^4\left(\frac{\mathcal{C}}{\mathcal{C}_0}\right) \tag{3.47}$$

is the dynamic shear viscosity of the ice cover, and

$$\dot{\gamma}_{ik} = \tfrac{1}{2} \left(\frac{\partial u_i^\infty}{\partial x_k} + \frac{\partial u_k^\infty}{\partial x_i} \right) \tag{3.48}$$

is the rate-of-strain tensor. It is apparent that η depends strongly on $\mathcal{H}(\boldsymbol{x}, t)$ and $\mathcal{C}(\boldsymbol{x}, t)$. The momentum balance equation now becomes

$$\frac{\mathcal{D}\boldsymbol{u}^\infty}{\mathcal{D}t} = -\frac{1}{\rho} \, \nabla_{\boldsymbol{x}} \Pi + \frac{1}{m} \, (\boldsymbol{F}_a - \boldsymbol{F}_o + \boldsymbol{F}_G + \boldsymbol{F}_H) - 2 \, \Omega_0 \, \boldsymbol{k} \times \boldsymbol{u}^\infty + \frac{1}{\rho} \, \nabla_{\boldsymbol{x}} \cdot \left(\eta \, \dot{\boldsymbol{\gamma}} \right). \tag{3.49}$$

This completes the development of our continuum theory.

4. Results

We shall now compare our theoretical results – both at the floe and continuum scales – with observations and simulations. Setting up and solving a canonical problem has, in our case, the disadvantage that there are no appropriate laboratory experiments to compare the results with. For this reason, we have to rely on results from observational data analyses (Rampal *et al.* 2009) and large-scale simulations of sea ice circulation in the Arctic performed using Newtonian rheology (Rothrock 1975*a*).

4.1. *Marginal distributions*

We begin with the PDFs of velocity fluctuations. The marginal equilibrium distributions, $\mathcal{P}_{u'}$ and $\mathcal{P}_{v'}$, are obtained from the joint distribution (3.35) using

$$\mathcal{P}_{u'} = \int_{-\infty}^{\infty} \mathcal{P}^{(0)}(u', v') \, \mathrm{d}v' = \frac{\rho \, \Lambda^2}{2 \, \pi} \int_{-\infty}^{\infty} \exp\left(-\Lambda \, \sqrt{u'^2 + v'^2} \right) \mathrm{d}v', \tag{4.1}$$

and

$$\mathcal{P}_{v'} = \int_{-\infty}^{\infty} \mathcal{P}^{(0)}(u', v') \, \mathrm{d}u' = \frac{\rho \, \Lambda^2}{2 \, \pi} \int_{-\infty}^{\infty} \exp\left(-\Lambda \, \sqrt{u'^2 + v'^2} \right) \mathrm{d}u'. \tag{4.2}$$

The integrals in (4.1) and (4.2) cannot be evaluated to give analytical expressions for $P_{u'}$ and $P_{v'}$, so we determine them numerically. The components u' and v' enter (3.24) as the fluctuating speed $V' = \sqrt{u'^2 + v'^2}$. This makes obtaining the PDF for the fluctuating speed, $\mathcal{P}_{V'}$, straightforward, which is found to be

$$\mathcal{P}_{V'} = \rho \, \Lambda^2 \, V' \, \exp\left(-\Lambda \, V' \right). \tag{4.3}$$

For the purpose of comparing $\mathcal{P}_{u'}$, $\mathcal{P}_{v'}$ and $\mathcal{P}_{V'}$ with observations, we assume that ρ is constant.

We use results from the analysis of the International Arctic Buoy Program data by Rampal *et al.* (2009). A total of 450 drifters deployed between 1979 and 2001 were used, and data from only those buoys whose positions were at least 100 km away from the coasts
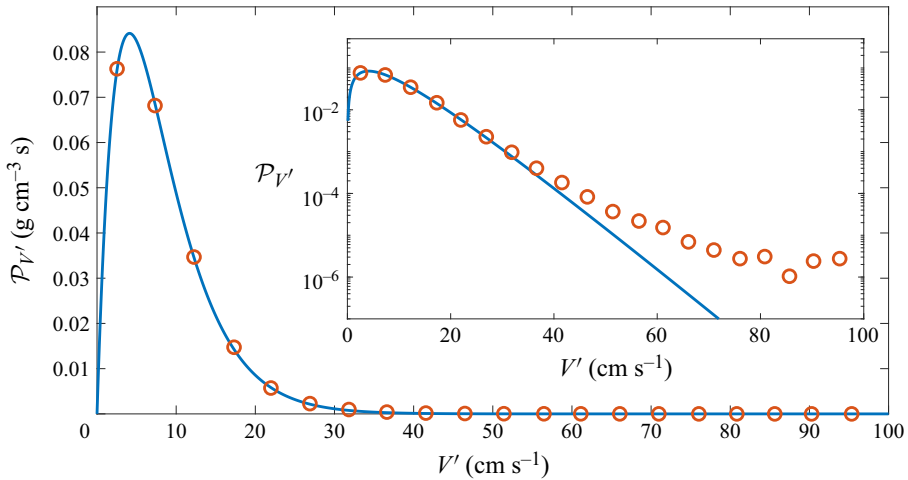
Figure 3. Comparison of our theoretical PDF for the fluctuating speed with observations. Circles are data from figure 10 in Rampal *et al.* (2009) and the solid curve is the functional form of the solution from theory (4.3). The value of ρ and Λ obtained from the fit are $0.94\,\mathrm{g\,cm^{-2}}$ and $0.238\,(\mathrm{cm\,s^{-1}})^{-1}$, respectively. The inset shows the same figure in log–linear plot.

were chosen. Rampal *et al.* (2009) chose a two-dimensional Cartesian coordinate system centred at the North Pole, with one of the axes pointing along the Greenwich meridian. For the analysis, the time period for winter was chosen from November to mid-May, and for summer from mid-June to mid-September. Further details on the procedure used to obtain the mean velocity, including the choice of length and time scales for averaging, and the velocity fluctuations can be found in Rampal *et al.* (2009).

In figure 3 we show the comparison between the theoretical PDF for the fluctuating speed and the observational PDF from Rampal *et al.* (2009). The functional form of the solution (4.3) is fit to the observational data, and ρ and Λ, which are the only fitting parameters, are determined from this fit. The values obtained are $\rho = 0.94\,\mathrm{g\,cm^{-2}}$ and $\Lambda = 0.24\,(\mathrm{cm\,s^{-1}})^{-1}$. The value of ρ obtained here is substantially smaller than the one used in the simulations of Rothrock (1975*a*,*b*) ($\rho = 300\,\mathrm{g\,cm^{-2}}$).

Using these values of ρ and Λ we compute the integral in (4.1) numerically to determine $\mathcal{P}_{u'}$. Noting that $\mathcal{P}_{u'}$ and $\mathcal{P}_{v'}$ have the same functional forms (4.1) and (4.2), we compare $\mathcal{P}_{u'}$ with observations and find that $\mathcal{P}_{u'}$ and $\mathcal{P}_{v'}$ for the velocity components are again Laplace distributions. This is shown in figure 4. As noted by Rampal *et al.* (2009), it is remarkable that the PDFs for u' and v' are approximately the same in each season, showing the fluctuations are isotropic and stationary.

The agreement between theory and observations seen in figures 3 and 4 provides confidence in our mean field theory. The modelling of the floe–floe interactions using a Coulomb friction term makes the floe exhibit a stick-slip behaviour in its dynamics (Elmer 1997; de Gennes 2005). This is similar in some aspects to the 'crack-slip' behaviour suggested by Thorndike (1986).

While the mean field theory has its advantages, it also has its limitations: the theory cannot explain the flattened tails in the PDF of speed (figure 3) and the marginal distributions (figure 4). One can speculate that this might be due to the advection of floes into a region of lower ice concentration or mean thickness or both. Incorporating such details when comparing results with observations is difficult. One can only infer the value of f/D from the fit, but determining f and D separately would require further analysis of
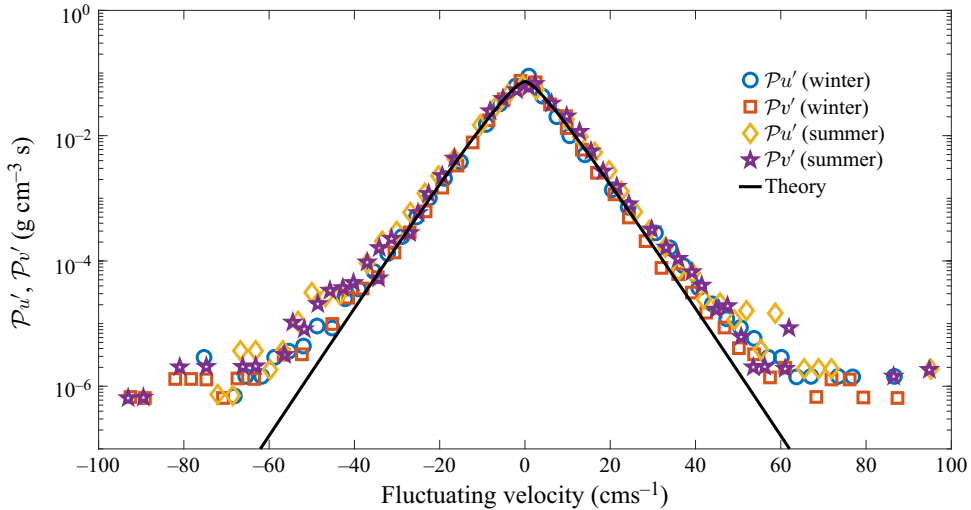
Figure 4. Comparison of our theoretical PDFs for ice velocity fluctuations with observations. Symbols are data from figure 9 in Rampal *et al.* (2009) and the solid curve is the PDF obtained from (4.1) after numerically evaluating the integral. The value of ρ and Λ used are $0.94 \, \mathrm{g \, cm}^{-2}$ and $0.238 \, (\mathrm{cm \, s}^{-1})^{-1}$, respectively (see figure 3).

the wind stress and ice field data to determine $\mathcal{C}$, $\mathcal{H}$ and $\mathcal{B}$, which is beyond the scope of the current work.

4.2. *Sea ice rheology*

Some of the previously developed viscous models of sea ice did not contain a pressure term, with the challenge lying in relating the pressure to the state of the ice cover (Rothrock 1970). Our approach allows us to determine explicitly the dependence of ice pressure and shear viscosity on the state of the ice cover. Here, we will explore these dependences in more detail.

In the limits $\mathcal{H} \to 0$ and/or $\mathcal{C} \to 0$ both pressure, Π, and viscosity, η, diverge, which is unphysical. This is because the continuum theory is not valid in the limit of vanishing ice cover. However, the motion of isolated ice floes in this limit can still be studied using the kinetic theory developed in § 2. For this reason, we are interested in the dynamics of a near complete ice cover. We take $\mathcal{C} \in [0.8, 1]$ which gives $\coth(\mathcal{C}/\mathcal{C}_0) = 1$. Thus, the only relevant variable for the state of the ice cover now is $\mathcal{H}$.

4.2.1. *Pressure*
The pressure field in sea ice is now given by

$$\Pi(\boldsymbol{x}, t) = \frac{3 \, \rho(\boldsymbol{x}, t)}{2} \, \frac{D^2}{f_0^2} \left[\exp\left(\frac{\mathcal{H}(\boldsymbol{x}, t)}{\mathcal{H}_0} \right) - 1 \right]^{-2}. \tag{4.4}$$

It is seen that as $\mathcal{H}$ increases the pressure decreases, but it increases with increasing ρ. This variation of Π with $\mathcal{H}$ is counterintuitive, but becomes clearer with the following, rather crude, analogy. In a dilute gas, the pressure in the gas (Π_g) depends on the density (ρ_g) and temperature (T_g) of the gas as (Harris 1971)
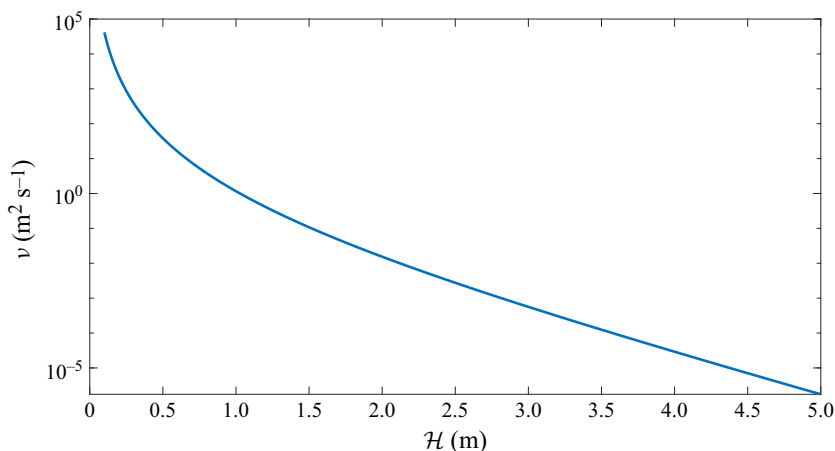
$$\Pi_g = \rho_g \, R T_g, \tag{4.5}$$

Figure 5. The dependence of kinematic viscosity, $\nu = \eta/\rho$, on the mean thickness, $\mathcal{H}$, based on the expression 4.6 for $D = 1$ m^2 s^{-3} and $f_0 = 1$ m s^{-2} .

which is the ideal gas law, with the gas constant R. Comparing (4.5) and (4.4) we see that for a fixed D, $\mathcal{H}$ determines the mobility of sea ice – the smaller the value of $\mathcal{H}$ the more mobile the ice floes are and hence larger the pressure will be because of increased number of collisions. Hence, $\mathcal{H}$ determines the pressure in sea ice like T_g determines the pressure in an ideal gas. This analogy is apt only because of similar mechanisms of 'microscopic' interactions in a gas and sea ice: (elastic) collisions between molecules in the former and (inelastic) collisions between floes in the latter.

4.2.2. *Shear viscosity*

The kinematic viscosity of sea ice, $\nu = \eta/\rho$, is

$$\nu = \frac{15\,D^3}{16\,f_0^4} \left[\exp\left(\frac{\mathcal{H}}{\mathcal{H}_0} \right) - 1 \right]^{-4}. \tag{4.6}$$

To highlight the dependence of ν on $\mathcal{H}$ we fix the constants $D = 1$ m^2 s^{-3} and $f_0 = 1$ m s^{-2} . The variation in ν with $\mathcal{H}$ is shown in figure 5. We see that ν varies by $O(10^{10})$ as the mean thickness varies from 0.1 to 5 m. This behaviour is again explained using the analogy with a dilute gas, as an increased mobility at smaller $\mathcal{H}$ means larger momentum transfer between different regions.

In the Arctic basin, the mean thickness is larger closer to the boundaries of the basin because of ridging (Kwok *et al.* 2009; Kwok & Cunningham 2015). Hence, the result from our theory implies that the viscosity of sea ice increases as one moves from the boundary regions to the interior of the basin. This explains why previous numerical studies found that a large value of shear viscosity, $\eta = 10^{12}$ kg s^{-1}, was required to generate sufficient stresses in the interior of the basin, but a smaller value of $\eta = 6 \times 10^9$ kg s^{-1} was required to observe realistic drift of sea ice and the formation of shear zones near the boundaries (Rothrock 1975*a,b*). This conflict over the choice of the value of η (or ν) is resolved through its dependence on $\mathcal{H}$, which has been found here. Hence, our theory is able to provide a qualitative explanation for the behaviour observed in the large-scale simulations, but a more detailed analysis of observational data are required to determine the quantitatively correct values of shear viscosity.

5. Summary and discussion

In summary, we have studied the motion of the Arctic sea ice cover at both the floe and continuum scales. We first considered the motion of a single ice floe and developed a mean field theory for its interactions with the neighbouring floes, neglecting phase change and ridging and rafting processes. The only variables used to represent the neighbouring floes were the ice concentration and the mean thickness. We assumed that only jostling and shearing modes of interaction drove the system towards local equilibrium and used a Coulomb friction term (Elmer 1997) to model the force resulting from these interactions. Using the Langevin equation for the floe velocity, we obtained the corresponding KCE for the PDF of the floe's velocity. A Chapman–Enskog analysis of this equation led to the continuum equations of motion and a viscous rheology that emerged from the floe scale dynamics. The pressure in the ice cover and the shear viscosity were found to depend strongly on the mean thickness.

To compare our theory with observations, we obtained the marginal distributions and the PDF for the fluctuating speed of the floe. The marginal distributions were found to be the Laplace distribution, in good qualitative agreement with observations (Rampal *et al.* 2009). We then placed our viscous model in the context of previous large-scale simulations of the ice cover (Rothrock 1975*a*) and were able to provide an explanation for some of the conflicting aspects of those studies. The qualitative agreement with observations and the large-scale simulations, despite the many simplifying assumptions made, provides confidence that our formulation of the problem is physically sound, and that the theory captures the leading-order physics associated with the motion of the ice cover.

An important aspect of the model that needs highlighting is that the interactions at the floe scale were modelled using a Coulomb friction term which is the simplest representation of plastic behaviour (Mellor 2013): if the floe comes to rest, then there is a certain minimum force – given by the threshold $\mathcal{F}$ – that needs to be applied to the floe to set it in motion again. However, this plastic-like behaviour at the floe scale still leads to the viscous rheology in the continuum limit. Although the viscous models developed in the past could not determine the dependence of pressure and viscosity on the state of the ice cover, our approach allows us to do this. In building our model we assumed that the ice floes always existed, but this is not always the case. Under the action of wind and ocean stresses the continuous ice cover fractures into floes, and recent theoretical and modelling efforts have focussed on modelling this process (Girard *et al.* 2011; Bouillon & Rampal 2015; Dansereau *et al.* 2016). This suggests that the sea ice rheology on shorter time scales is perhaps the brittle rheology, but on much longer time scales it is viscous: the ice cover fractures into floes at shorter time scales (Asplin *et al.* 2012) and once the floes are produced the momentum transfer happens through shearing and jostling between the floes, as suggested by Reed & Campbell (1962). This description provides a qualitative picture of the response of the ice cover over short and long time scales. However, this picture is not accurate during the early part of the freezing season when smaller floes coagulate to form larger floes and subsequently a continuous ice cover (Weeks & Ackley 1986).

The relative simplicity of our approach has both advantages and limitations. The first advantage is that from a detailed study of the motion of a single floe it is possible to obtain the large-scale behaviour of the ice cover. This provides an answer to one of the longstanding questions of how the rheological properties of a viscous model relate to the variables that quantify the state of the ice cover (Rothrock 1975*a*; Untersteiner 1986). The second advantage is that it allows for analytical tractability, which leads to the explicit continuum equations starting from the floe dynamics. The last advantage is

that it provides unambiguous results, with only two free parameters, that can be compared with observations. This allows for the improvement of the model with relative ease when compared with most other models that do not have a similar floe-scale picture associated with them. Our theory also provides an observationally consistent framework to study the statistical properties of the ice velocity field, which would help in the development of simplified mathematical models of sea ice motion for incorporation into climate models.

The limitations of the theory are the following. First, the theory does not take into account the thermal growth and mechanical deformations of the ice floe. This is remedied by writing the mass of the ice floe as $m = \rho_i \, \pi \, R^2 \, h$, where ρ_i is the constant density of the ice floe, and rewriting (2.2) as

$$m \frac{\mathrm{d}\boldsymbol{v}}{\mathrm{d}t} = -\boldsymbol{v} \frac{\mathrm{d}m}{\mathrm{d}t} + \boldsymbol{F}_a + \mathcal{B} \, \boldsymbol{\xi}(t) - \boldsymbol{F}_o + \boldsymbol{F}_G + \boldsymbol{F}_H - 2 \, m \, \Omega_0 \, \boldsymbol{k} \times \boldsymbol{v} - \mathcal{F} \, \boldsymbol{S}(\boldsymbol{v} - \boldsymbol{u}^\infty).$$

(5.1)

The changes in $R(t)$ and $h(t)$ can now be coupled with the momentum equation (5.1). This, however, leads to a six-dimensional Fokker–Planck equation which is challenging to solve – both analytically and numerically. The second limitation is that some of the key parameters in the theory, such as D and f_0, cannot be determined without a detailed analysis of observational data.

These limitations, however, are not severe and can be overcome by solving the coupled stochastic differential equations for $\boldsymbol{v}$ and h and by performing a detailed, pan-Arctic analysis of wind stress and thickness distribution data. Our previous work on the thickness distribution of sea ice (Toppaladoddi & Wettlaufer 2015, 2017; Toppaladoddi *et al.* 2023) and our current theory provide a physical and mathematical framework to achieve this.

REFERENCES

AGARWAL, S. & WETTLAUFER, J.S. 2017 The statistical properties of sea ice velocity fields. *J. Clim.* **30** (13), 4873–4881.

AGARWAL, S. & WETTLAUFER, J.S. 2018 Fluctuations in Arctic sea-ice extent: comparing observations and climate models. *Phil. Trans. R. Soc. A* **376** (2129), 20170332.

ASPLIN, M.G., GALLEY, R., BARBER, D.G. & PRINSENBERG, S. 2012 Fracture of summer perennial sea ice by ocean swell as a result of Arctic storms. *J. Geophys. Res.-Oceans* **117**, C06025.

BOUCHAT, A. 2022 Sea ice rheology experiment (SIREx): 1. Scaling and statistical properties of sea-ice deformation fields. *J. Geophys. Res.-Oceans* **127** (4), e2021JC017667.

BOUILLON, S. & RAMPAL, P. 2015 Presentation of the dynamical core of neXtSIM, a new sea ice model. *Ocean Model.* **91**, 23–37.

CAMPBELL, W.J. 1965 The wind-driven circulation of ice and water in a polar ocean. *J. Geophys. Res.* **70** (14), 3279–3301.

CHANDRASEKHAR, S. 1943 Stochastic problems in physics and astronomy. *Rev. Mod. Phys.* **15** (1), 1–89.

CHAPMAN, S. & COWLING, T.G. 1990 *The Mathematical Theory of Non-Uniform Gases*. Cambridge University Press.

COLONY, R. & THORNDIKE, A.S. 1984 An estimate of the mean field of Arctic sea ice motion. *J. Geophys. Res.-Oceans* **89** (C6), 10623–10629.

COLONY, R. & THORNDIKE, A.S. 1985 Sea ice motion as a drunkard's walk. *J. Geophys. Res.-Oceans* **90** (C1), 965–974.

COON, M.D., MAYKUT, G.A., PRITCHARD, R.S., ROTHROCK, D.A. & THORNDIKE, A.S. 1974 Modeling the ice pack as an elastic-plastic material. *AIDJEX Bull.* **24**, 1–106.

DA CRUZ, F., EMAM, S., PROCHNOW, M., ROUX, J.-N. & CHEVOIR, F. 2005 Rheophysics of dense granular materials: discrete simulation of plane shear flows. *Phys. Rev. E* **72** (2), 021309.

DAMSGAARD, A., ADCROFT, A. & SERGIENKO, O. 2018 Application of discrete element methods to approximate sea ice dynamics. *J. Adv. Model. Earth Syst.* **10** (9), 2228–2244.

DAMSGAARD, A., SERGIENKO, O. & ADCROFT, A. 2021 The effects of ice floe-floe interactions on pressure ridging in sea ice. *J. Adv. Model. Earth Syst.* **13** (7), e2020MS002336.

DANSEREAU, V., WEISS, J., SARAMITO, P. & LATTES, P. 2016 A Maxwell elasto-brittle rheology for sea ice modelling. *Cryosphere* **10** (3), 1339–1359.

DE DIEGO, G.G., GUPTA, M., GERING, S.A., HARIS, R. & STADLER, G. 2024 Modelling sea ice in the marginal ice zone as a dense granular flow with rheology inferred from discrete element model data. *J. Fluid Mech.* **1000**, A22.

DOERING, C.R. 2018 Modeling complex systems: stochastic processes, stochastic differential equations, and Fokker-Planck equations. In *1990 Lectures in Complex Systems*, pp. 3–52. CRC Press.

ELMER, F.-J. 1997 Nonlinear dynamics of dry friction. *Phys. A Math. Gen.* **30** (17), 6057–6063.

EVANS, R.J. 1970 Notes on a possible constitutive law for Arctic sea ice. *AIDJEX Bull.* **2**, 13–17.

EVANS, R.J. & UNTERSTEINER, N. 1971 Thermal cracks in floating ice sheets. *J. Geophys. Res.* **76** (3), 694–703.

FELTHAM, D.L. 2008 Sea ice rheology. *Annu. Rev. Fluid Mech.* **40** (1), 91–112.

FELTHAM, D.L. 2005 Granular flow in the marginal ice zone. *Phil. Trans. R. Soc. A* **363** (1832), 1677–1700.

FOX-KEMPER, B. 2021 Climate change 2021: the physical science basis. In *Contribution of Working Group I to the Sixth Assessment Report of the Intergovernmental Panel On Climate Change, Chap. Ocean, Cryosphere and Sea Level Change*. Cambridge University Press.

DE GENNES, P.-G. 2005 Brownian motion with dry friction. *J. Stat. Phys.* **119** (5), 953–962.

GIRARD, L., BOUILLON, S., WEISS, J., AMITRANO, D., FICHEFET, T. & LEGAT, V. 2011 A new modeling framework for sea-ice mechanics based on elasto-brittle rheology. *Ann. Glaciol.* **52** (57), 123–132.

GOLDREICH, P. & TREMAINE, S. 1978 The velocity dispersion in Saturn's rings. *Icarus* **34** (2), 227–239.

GRAD, H. 1958 Principles of the kinetic theory of gases. In *Thermodynamics of Gases*, pp. 205–294. Springer.

DE GROOT, S.R. & MAZUR, P. 2013 *Non-Equilibrium Thermodynamics*. Courier Corporation.

HARRIS, S. 1971 *An Introduction to the Theory of the Boltzmann Equation*. Dover.

HAYAKAWA, H. 2005 Langevin equation with Coulomb friction. *Phys. D: Nonlinear Phenom.* **205** (1-4), 48–56.

HERMAN, A. 2011 Molecular-dynamics simulation of clustering processes in sea-ice floes. *Phys. Rev. E* **84** (5), 056104.

HERMAN, A. 2013 Numerical modeling of force and contact networks in fragmented sea ice. *Ann. Glaciol.* **54** (62), 114–120.

HERMAN, A. 2016 Discrete-element bonded-particle sea ice model design, version 1.3 a–model description and implementation. *Geosci. Model Dev.* **9** (3), 1219–1241.

HERMAN, A. 2017 Wave-induced stress and breaking of sea ice in a coupled hydrodynamic discrete-element wave–ice model. *Cryosphere* **11** (6), 2711–2725.

HERMAN, A. 2022 Granular effects in sea ice rheology in the marginal ice zone. *Phil. Trans. R. Soc. A* **380** (2235), 20210260.

HIBLER, W.D. 1977 A viscous sea ice law as a stochastic average of plasticity. *J. Geophys. Res.* **82** (27), 3932–3938.

HIBLER, W.D. 1979 A dynamic thermodynamic sea ice model. *J. Phys. Oceanogr.* **9** (4), 815–846.

HOPKINS, M.A. 1996 On the mesoscale interaction of lead ice and floes. *J. Geophys. Res.-Oceans* **101** (C8), 18315–18326.

HOPKINS, M.A. & THORNDIKE, A.S. 2006 Floe formation in Arctic sea ice. *J. Geophys. Res.-Oceans* **111**, C11S23.

HOWELL, P., KOZYREFF, G. & OCKENDON, J. 2009 *Applied Solid Mechanics*. Cambridge University Press.

HUNKE, E.C. & DUKOWICZ, J.K. 1997 An elastic–viscous–plastic model for sea ice dynamics. *J. Phys. Oceanogr.* **27** (9), 1849–1867.

HUTTER, N. 2022 Sea ice rheology experiment (SIREx): 2. Evaluating linear kinematic features in high-resolution sea ice simulations. *J. Geophys. Res.: Oceans* **127** (4), e2021JC017666.

KEEN, A. 2021 An inter-comparison of the mass budget of the Arctic sea ice in CMIP6 models. *Cryosphere* **15** (2), 951–982.

KRAMERS, H.A. 1940 Brownian motion in a field of force and the diffusion model of chemical reactions. *Physica* **7** (4), 284–304.

KWOK, R. & CUNNINGHAM, G.F. 2015 Variability of Arctic sea ice thickness and volume from CryoSat-2. *Phil. Trans. R. Soc. A* **373** (2045), 20140157.

KWOK, R., CUNNINGHAM, G.F., WENSNAHAN, M., RIGOR, I., ZWALLY, H.J. & YI, D. 2009 Thinning and volume loss of the Arctic Ocean sea ice cover: 2003–2008. *J. Geophys. Res.-Oceans* **114**, C07005.

KWOK, R. & UNTERSTEINER, N. 2011 The thinning of Arctic sea ice. *Phys. Today* **64** (4), 36–41.

LEBOWITZ, J.L., FRISCH, H.L. & HELFAND, E. 1960 Nonequilibrium distribution functions in a fluid. *Phys. Fluids* **3** (3), 325–338.

LIFSHITZ, E.M. & PITAEVSKII, L.P. 2005 *Physical Kinetics*. Butterworth-Heinemann.

MANUCHARYAN, G.E. & MONTEMURO, B.P. 2022 Subzero: a sea ice model with an explicit representation of the floe life cycle. *J. Adv. Model. Earth Syst.* **14** (12), e2022MS003247.

MAXWELL, J.C. 1860 On the motions and collisions of perfectly elastic spheres. *Lond. Edin. Phil. Mag. & J. Sci.* **19** (124), 19–32.

MELLOR, M. 2013 Mechanical behavior of sea ice. In *The Geophysics of Sea Ice*, (ed. N. UNTERSTEINER), pp. 165–281. Springer.

NYE, J.F. 1973 Is there any physical basis for assuming linear viscous behavior for sea ice? *AIDJEX Bull.* **21**, 18–19.

ÓLASON, E., BOUTIN, G., KOROSOV, A., RAMPAL, P., WILLIAMS, T., KIMMRITZ, M., DANSEREAU, V. & SAMAKÉ, A. 2022 A new brittle rheology and numerical framework for large-scale sea-ice models. *J. Adv. Model. Earth Syst.* **14** (8), e2021MS002685.

PARMERTER, R.R. 1975 A model of simple rafting in sea ice. *J. Geophys. Res.* **80** (15), 1948–1952.

PARMERTER, R.R. & COON, M.D. 1972 Model of pressure ridge formation in sea ice. *J. Geophys. Res.* **77** (33), 6565–6575.

RAMPAL, P., WEISS, J., DUBOIS, C. & CAMPIN, J.-M. 2011 IPCC climate models do not capture Arctic sea ice drift acceleration: consequences in terms of projected sea ice thinning and decline. *J. Geophys. Res.-Oceans* **116**, C00D07.

RAMPAL, P., WEISS, J., MARSAN, D. & BOURGOIN, M. 2009 Arctic sea ice velocity field: general circulation and turbulent-like fluctuations. *J. Geophys. Res.-Oceans* **114**, C10014.

REED, R.J. & CAMPBELL, W.J. 1962 The equilibrium drift of ice station Alpha. *J. Geophys. Res.* **67** (1), 281–297.

REIF, F. 1965 *Fundamentals of Statistical and Thermal Physics*. McGraw-Hill.

RISKEN, H. 1996 *Fokker-Planck Equation*. Springer.

ROTHROCK, D.A. 1970 The pressure term in the constitutive law of an ice pack. *AIDJEX Bull.* **2**, 28–32.

ROTHROCK, D.A. 1975*a* The mechanical behaviour of pack ice. *Annu. Rev. Earth Planet Sci.* **3** (1), 317–342.

ROTHROCK, D.A. 1975*b* The steady drift of an incompressible Arctic ice cover. *J. Geophys. Res.* **80** (3), 387–397.

ROTHROCK, D.A. & THORNDIKE, A.S. 1984 Measuring the sea ice floe size distribution. *J. Geophys. Res.-Oceans* **89** (NC4), 6477–6486.

SHEN, H.H., HIBLER, W.D. & LEPPÄRANTA, M. 1987 The role of floe collisions in sea ice rheology. *J. Geophys. Res.-Oceans* **92** (C7), 7085–7096.

SOLOMON, H. 1970 A study of ice dynamics relevant to AIDJEX. *AIDJEX Bull.* **2**, 33–50.

STEELE, M., MORISON, J.H. & UNTERSTEINER, N. 1989 The partition of air-ice-ocean momentum exchange as a function of ice concentration, floe size, and draft. *J. Geophys. Res.-Oceans* **94** (C9), 12739–12750.

SVERDRUP, H.U. 1928 The wind-drift of the ice on the northern siberian shelf. In *the Norwegian North Polar Expedition with the Maud: Scientific Results*, vol. 4, pp. 1–46.

THORNDIKE, A.S. 1986 Diffusion of sea ice. *J. Geophys. Res.-Oceans* **91** (C6), 7691–7696.

THORNDIKE, A.S. & COLONY, R. 1982 Sea ice motion in response to geostrophic winds. *J. Geophys. Res.-Oceans* **87** (C8), 5845–5852.

THORNDIKE, A.S., ROTHROCK, D.A., MAYKUT, G.A. & COLONY, R. 1975 The thickness distribution of sea ice. *J. Geophys. Res.* **80** (33), 4501–4513.

TIMOKHOV, L.A. 1970 One-dimensional stochastic ice drift. *AIDJEX Bull.* **3**, 80–93.

TOPPALADODDI, S., MOON, W. & WETTLAUFER, J.S. 2023 Seasonal evolution of the sea ice thickness distribution. *J. Geophys. Res.-Oceans* **128** (5), e2022JC019540.

TOPPALADODDI, S. & WETTLAUFER, J.S. 2015 Theory of the sea ice thickness distribution. *Phys. Rev. Lett.* **115** (14), 148501.

TOPPALADODDI, S. & WETTLAUFER, J.S. 2017 Statistical mechanics and the climatology of the Arctic sea ice thickness distribution. *J. Stat. Phys.* **167** (3-4), 683–702.

TSAMADOS, M., FELTHAM, D.L. & WILCHINSKY, A.V. 2013 Impact of a new anisotropic rheology on simulations of arctic sea ice. *J. Geophys. Res.-Oceans* **118** (1), 91–107.

UHLENBECK, G.E. & ORNSTEIN, L.S. 1930 On the theory of the Brownian motion. *Phys. Rev.* **36** (5), 823–841.

UNTERSTEINER, N. 1986 The geophysics of sea ice: overview. In *The Geophysics of Sea Ice* (ed. N. Untersteiner), pp. 1–8. Springer.

VELLA, D. & WETTLAUFER, J.S. 2008 Explaining the patterns formed by ice floe interactions. *J. Geophys. Res.-Oceans* **113** (C11), C11011.

WEEKS, W.F. & ACKLEY, S.F. 1986 The growth, structure, and properties of sea ice. In *The Geophysics of Sea Ice* (ed. N. Untersteiner), pp. 9–164. Springer.

WEST, B., O'CONNOR, D., PARNO, M., KRACKOW, M. & POLASHENSKI, C. 2022 Bonded discrete element simulations of sea ice with non-local failure: applications to Nares Strait. *J. Adv. Model. Earth Syst.* **14** (6), e2021MS002614.

WILCHINSKY, A.V. & FELTHAM, D.L. 2004 A continuum anisotropic model of sea-ice dynamics. *Proc. R. Soc. A* **460** (2047), 2105–2140.

WYCOFF, D. & BALAZS, N.L. 1987 Multiple time scales analysis for the Kramers-Chandrasekhar equation with a weak magnetic field. *Physica A* **146** (1–2), 201–218.